# Three-Dimensional Fusion of Coronary Arteries with Myocardial Perfusion Distributions: Clinical Validation

Tracy L. Faber, PhD[1]; Cesar A. Santana, MD, PhD[1]; Ernest V. Garcia, PhD[1]; Jaume Candell-Riera, MD[2]; Russell D. Folks, BS[1]; John W. Peifer, MS[3]; Andrew Hopper, BS[4]; Santiago Aguade, MD[2]; Joan Angel, MD[2]; and J. Larry Klein, MD[4]

[1]Department of Radiology, Emory University, Atlanta, Georgia; [2]Hospital Universitari Vall d' Hebron, Barcelona, Spain; [3]Biomedical Interactive Technology Center, Georgia Institute of Technology, Atlanta, Georgia; and [4]Atlanta Cardiology Group, Atlanta, Georgia

Clinical decisions regarding diagnosis and effective treatment of coronary artery disease frequently require integration of information from various imaging modalities, which are acquired, processed, and read at different physical locations and times. We have developed methods to integrate the information in 2 cardiac imaging studies, perfusion SPECT and coronary angiography. Three-dimensional (3D) models of the coronary artery tree created from biplane angiograms were automatically aligned with 3D models of the left ventricular epicardial surface created from perfusion SPECT. Myocardial mass at risk was used as a unique measure to validate the accuracy of the unification. **Methods:** Thirty patients were injected with the perfusion agent $^{99m}$Tc-tetrosfosmin during balloon occlusion while undergoing percutaneous transluminal coronary angioplasty for single-vessel coronary artery disease. Thus, a single, severe perfusion defect was induced by a single coronary artery occlusion of known severity and placement. The accuracy of the unification was measured by computing the overlap between physiologic area at risk, determined using SPECT perfusion quantification techniques only, and anatomic area at risk, determined using coronary artery anatomy aligned with the epicardial surface of the left ventricle. **Results:** The unification resulted in an 80% overlap of areas at risk, and an overlap of 84% of normal areas, for all coronary artery distributions. The mass at risk measured based on the unified anatomic information correlated with the physiologically based mass at risk as $y = 0.92x + 10.3$ g; $r = 0.76$, SEE = 10.4 g. **Conclusion:** A unification algorithm for automatically registering 3D models of the epicardial surface from perfusion SPECT and 3D coronary artery trees from coronary angiography has been presented and validated in 30 patient studies.

**Key Words:** image fusion; mass at risk; myocardial perfusion SPECT; coronary arteriography

**J Nucl Med 2004; 45:745–753**

Clinical decisions regarding diagnosis and effective treatment of coronary artery disease frequently require integration of information from various imaging modalities. The existence and severity of coronary artery blockage are evaluated using coronary angiography. Nuclear cardiology studies of myocardial perfusion—specifically, SPECT—are used to observe the physiologic sequelae of coronary artery stenosis. Both pieces of information are then combined to determine appropriate treatment.

In current clinical practice, the cardiologist subjectively performs the integration of anatomic and physiologic information from angiograms and SPECT perfusion images. Frequently, the two image sets are viewed independently and, most often, in 2 dimensions, as demonstrated in Figures 1A and 1B. The physician mentally combines information about coronary artery blockages from the angiograms with that of cardiac perfusion from SPECT. However, the 2-dimensional (2D) nature of coronary angiography, in which the angiograms are actually projection images, combined with the slice-by-slice display of cardiac perfusion studies, makes subjective integration difficult. The location of a stenosis with respect to the left ventricular (LV) epicardial surface can only be judged approximately, and thus, its physiologic effects may be difficult to determine. The existence of more than one blocked artery exacerbates this problem, especially if the degree of stenosis is near 50%. Such stenoses may or may not cause perfusion abnormalities.

Recent advances in computer technology now allow 3-dimensional (3D) reconstruction of the coronary artery tree from biplane angiography, or even from 2 views obtained from single-plane angiography (1,2). In addition, the 3D LV epicardial surface can be modeled based on tomographic perfusion studies (3). These technologic improvements have enabled us to align or fuse objectively 3D models of the coronary anatomy with the myocardial physiology and then display the superimposition or fusion. This allows the locations of coronary stenoses and perfusion abnormalities to be
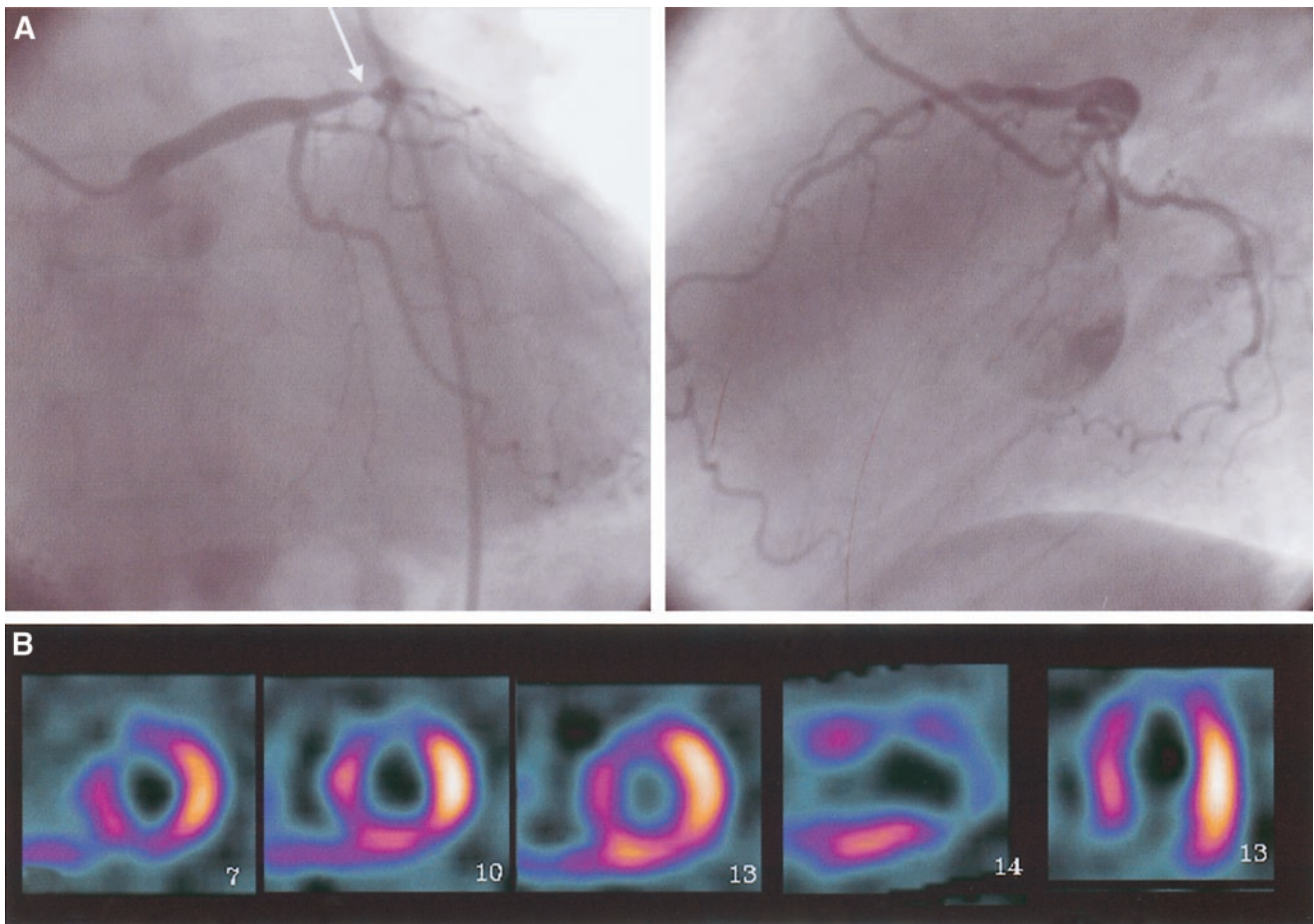
**FIGURE 1.** (A) Biplane coronary angiograms from patient with left anterior descending artery (LAD) stenosis. Location of stenosis is marked with arrow. (B) Original SPECT perfusion images of same patient as in A, with radionuclide injected during total balloon occlusion of LAD. SPECT images are serial short-axis slices taken from near the apex (left) through the basal left ventricular region (middle), vertical long-axis, and horizontal long-axis sections. A large perfusion abnormality is seen in anterior and septal walls of left ventricle.

explicitly visualized in 3 dimensions and helps relate the anatomic cause of a blocked artery with the physiologic effect of myocardial hypoperfusion. Although investigators have shown the clinical value of this type of 3D image fusion (4), no methodologic validation exists to date.

The purpose of this study was to assess the performance of this fusion in actual patient studies. We used a unique, specific patient population with single-vessel disease and no collateral vessels viewed during angiography in which a profound perfusion abnormality was induced by balloon occlusion during percutaneous transluminal coronary angioplasty (PTCA) of the single lesion. The perfusion abnormality was imaged by injecting a $^{99m}$Tc perfusion agent during the occlusion. Thus, the single coronary artery occlusion was the cause of the single perfusion defect, and the myocardial territory normally supplied by the arterial bed distal to the occlusion should correspond to the perfusion defect.

The myocardial area at risk predicted by coronary arteriography, or the anatomic area at risk, depends on the shape and extent of myocardium distal to the coronary artery occlusion, the anatomy of the coronary artery tree, the shape of the epicardial surface, and the unification between the 2 objects (5). If these are correct, then the anatomic area at risk should overlap the perfusion abnormality, or the physiologic area at risk. Previous work has shown the accuracy of 3D reconstruction of the coronary artery trees (1) and epicardial surfaces (3); thus, the overlap depends primarily on the accuracy of the fusion process. In this work, we measured overlap using estimates of myocardial mass to validate the fusion process.

## MATERIALS AND METHODS

### Patient Population

The study consisted of 30 nonconsecutive patients (26 men, 4 women; mean age, 61 ± 10 y) without previous myocardial infarction and with normal wall motion and normal baseline LV function who underwent elective PTCA for single-vessel disease. The indications for coronary angioplasty were either unstable angina ($n = 13$) or exertional angina ($n = 17$). All patients had normal baseline electrocardiograms. All patients received cardiac medications within 12 h of angioplasty; these comprised calcium channel antagonists in 16 patients, nitrates in 20, and β-adrenergic blocking agents in 17. The protocol was approved by the Ethical

Committee of Hospital Universitari Vall d'Hebron, and all patients signed informed consent.

## Angiography and Angioplasty

Coronary arteriography was performed using 1 of 2 Philips systems, Optimus M200 (biplane) or Integris (single plane). In all cases, a field of view of 17.8 cm was used, and the source-to-image intensifier distance was measured. Angiograms were recorded on 35-mm film for 15 patients and digitized; in the other 15 patients, angiograms were acquired digitally and saved on compact disks using dicom format. Example angiograms are shown in Figure 1A.

All patients received aspirin and ticlopidine at least 24 h before angioplasty. After intracoronary nitroglycerin injection, 2 orthogonal views were obtained. The views were selected to show the known stenosis, to assess collateral flow, and to widely display the coronary tree affected by the blockage. The balloon catheter was passed via the femoral artery over a steerable guide wire under fluoroscopy and inflated across the coronary lesion. After 10–15 s of balloon inflation, $^{99m}$Tc-tetrofosmin was injected into peripheral intravenous tubing; inflation was maintained for approximately 90 s to allow time for $^{99m}$Tc-tetrofosmin myocardial distribution. After that, further balloon inflations or stent deployments were performed to achieve revascularization to the myocardium.

## SPECT Acquisition and Processing

Occlusion and rest SPECT studies were performed on separate days, with an interval of >24 h. The occlusion study was performed approximately 1 h after tetrofosmin injection during PTCA; the rest study was acquired the following day. The same dose (800 MBq) was used for both studies. Patients were imaged 1 h after administration of the radiopharmaceutical using an Elscint SP4 scintillation camera with a high-resolution collimator. Sixty projections over 180° were acquired using a semicircular orbit starting at 30° right anterior oblique. Reconstructions were performed with a Butterworth filter of critical frequency 0.4 cycle/cm and order 5. Transaxial images were reformatted into standard short-axis, horizontal long-axis, and vertical long-axis sections. An example of the SPECT images obtained after injecting radiotracer during balloon occlusion is shown in Figure 1B.

## Creation of 3D Models for Unification

Methods to create 3D models of the epicardial surface from perfusion SPECT have been previously described and validated (3). Briefly, the myocardium is resampled at numerous angles about the LV long axis using a hybrid coordinate system whose origin is the long axis (6). At each sampling angle, the highest intensity point in the myocardium is detected; this point should lie close to the myocardial center. By assuming a constant myocardial thickness, the epicardial surface can be estimated by adding a fixed radius to the myocardial center points. Similarly, the endocardial surface can be modeled by subtracting this radius from the myocardial center points. Finally, the epicardial and endocardial boundary points can be connected into triangles to form polygonal epicardial and endocardial surfaces. Figure 2A shows the epicardial surfaces resulting from this approach in the same subject as shown in Figure 1.

Methods to generate 3D models of the coronary artery tree from biplane coronary angiograms have been previously described and validated (7,8). Briefly, 3D models were created by locating the artery center lines in 2 angiographic views and then using a triangulation method to reconstruct the original 3D object. The artery center lines were determined using a user-guided process.
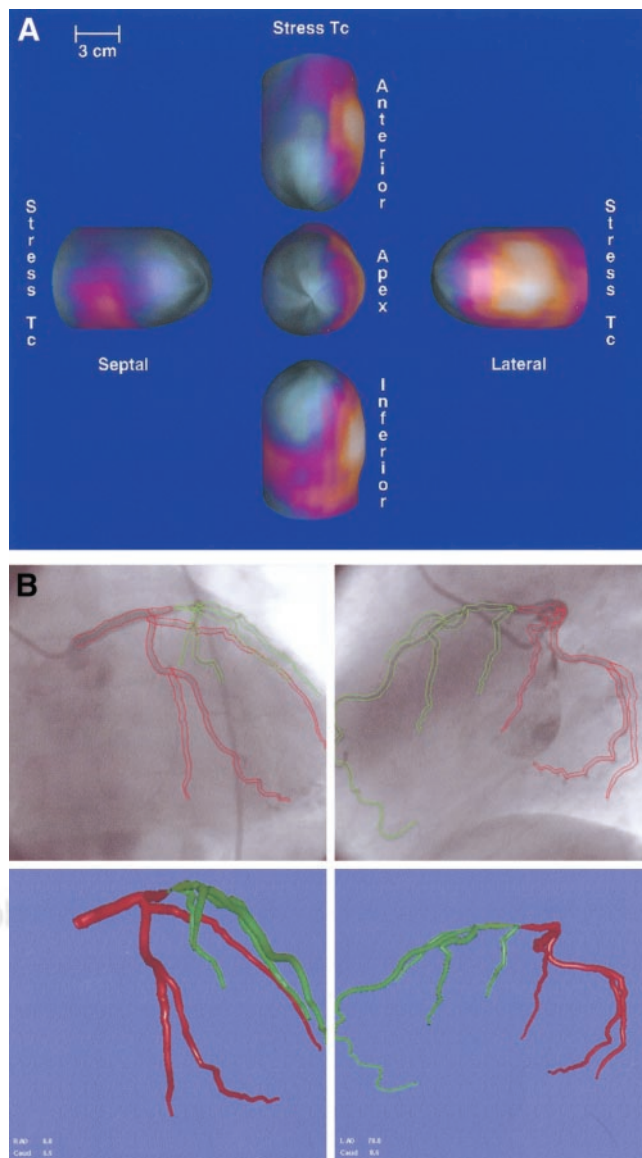


**FIGURE 2.** Three-dimensional models created from original images. (A) Five views of the 3D LV epicardial surface color coded for perfusion. These are 3D models corresponding to original images shown in Figure 1. Note perfusion defect in anteroseptal wall as represented by green and blue regions. (B) Three-dimensional left coronary artery tree (bottom right), created after boundary detection of arteries on angiograms (top left and right). Tree is color coded green distal to occlusion. This is same patient as shown in Figure 1.

The user moved the cursor in the general path of the coronary artery, and a computer algorithm followed the nearest low-intensity valley to the cursor. Once the center lines were detected in 2 angiographic views, the actual boundaries could be modeled by assuming a constant arterial radius or segmented using automatic edge-detection techniques—for example, that described by Reiber and Surruys (8). In this case, we used the fast, constant radius approach, since the exact diameter of the coronary arteries was less important for this analysis.

After the coronary arteries were thus segmented in both views, they were reconstructed into the 3D tree. This is described by

Peifer et al. (9). Essentially, the arteries are assumed to have a circular cross section computed as the average of the radius in the 2 views and, based on the precise geometry of the detector positions and angles, geometric triangulation can be used to reconstruct the 3D coronary artery tree. An example is shown in Figure 2B. Recent evaluations of the goodness of this approach are discussed in Klein et al. (1). Finally, the coronary artery trees were scaled to match the size of the LV models, using the known zoom factor of the angiograms and the pixel sizes of the SPECT image.

## Unification of 3D Models

The overall approach to unification of the coronary artery tree with the LV epicardial surface was one of optimization. The model of the 3D coronary arteries was matched with the model of the 3D epicardial surface by minimizing a cost function describing how the models are related. There were 3 separate steps for unification. First, the models were placed in a rough, approximate alignment. Then, an iterative algorithm was used to refine the registration. Finally, a nonlinear warping was applied to force the artery tree to lie exactly on the epicardial surface. All steps in the unification procedure were performed automatically with no user intervention.

## Initial Approximate Alignment

It is known that the course of the proximal left anterior descending artery (LAD) follows the anterior interventricular groove after it branches from the left main coronary artery. Likewise, the posterior descending artery (PDA) follows the posterior interventricular groove. This information can be used to provide a rough alignment of the coronary artery trees with the epicardial surface before applying the more time-consuming iterative closest point (ICP) algorithm. The anterior and inferior interventricular grooves were automatically detected from the short-axis image slices using a search algorithm (10). In this approach, circumferential samples were taken outside of the epicardial surface for 8 short-axis slices from the base to the apex. Changes in intensity between adjacent angles in each profile were computed, and a smooth line connecting maximal changes (where the profile samples moved from background into the right ventricular wall) was determined using a branch-and-bound search. The LAD was aligned with the anterior interventricular groove, and the coronary artery tree was rotated about the interventricular groove until the distance between the tree and epicardium was minimized. The same approach was used with the PDA and the inferior interventricular groove. This provided a reasonable starting position for either the left or right coronary artery (RCA) tree, after which the ICP algorithm could be applied.

## ICP Algorithm

Once the LV surface and coronary artery tree have been placed in an approximate alignment, the registration is refined using the ICP algorithm (11). ICP consists of 2 steps: (a) estimate correspondences between points on the arteries and the epicardial surface and (b) compute the transform to align the corresponding pairs of points—that is, for each point of the artery, the closest point on the epicardial surface model must be found. From the resulting couplets of corresponding points, the optimal translation and rotation that minimizes the mean square error between them can be computed. These 2 steps are iterated until an optimum is reached.

Our implementation of these 2 steps is new and unique, tuned to the problem, and designed to be both fast and accurate (10). For a given data point in the artery model, our algorithm returns the closest point on the LV epicardial surface by making use of geometric properties intrinsic to a convex surface, such as the LV epicardium, represented using spheric coordinates. Once all corresponding epicardial surface points have been found for each artery point, the optimal rigid transformation that minimizes the mean square distance between the point set is computed. The approach we use for computing this transformation is that described by Kim and Aggarwal (12).

The computed transformation is optimal for a certain set of artery/epicardium point pairs. But once the transformation is applied, the newly transformed artery points may correspond with different surface points. It is thus necessary to recompute the correspondences and the new optimal transformation iteratively. In this implementation, the iteration is continued until the mean distance between corresponding points does not decrease by >1% of the mean distance at the previous position, or for 100 iterations, whichever comes first. The optimal position found at the end of the loop depends on the initial position; it is a local minimum of the error function.

## Nonlinear Warping

The final step in unification was to warp the coronary artery trees so that they were placed exactly on the epicardial surface. This was performed by transforming the coronary artery points into the same hybrid coordinate system as the epicardial surface. Then, the distance between each coronary artery point and the LV surface could be easily computed. The coronary artery points were each translated by this distance so that they were congruent with the epicardium. More details of this operation are given in Peifer et al. (9).

## Computing Physiologic Mass at Risk

The resampling of the myocardium for surface detection in SPECT studies also serves as a basis for perfusion quantification. The details of this approach are given in Garcia et al. (6). Simply, the intensity of the myocardium at each sampling angle is compared with a database of normal values after normalization for injected dose and other image intensity variations. Areas that fall below the threshold for normal intensity can therefore be automatically identified. Stress and rest distributions can be thus quantified, and areas that are abnormal at either rest or stress can be identified. In a standard SPECT perfusion acquisition, areas that are abnormal at both rest and stress can be considered "fixed" defects; abnormalities at stress that significantly normalize at rest may be considered "reversible." Thus, reversible areas are currently viable, but "at risk" for myocardial infarction if the disease progresses. In perfusion quantification displays, fixed defects are shown as blacked-out regions, whereas reversible defects are shown as whited-out regions. Figure 3A shows the results of perfusion quantification on the same subject depicted in Figure 1.

In this work, because we were in essence "causing" a resting defect during PTCA, all areas of the myocardium that were quantified as abnormal for perfusion after the first injection of tetrofosmin were those that were at risk for myocardial infarction if the disease progressed. (Because these areas were revascularized, SPECT acquisitions obtained the following day showed that the entire area at risk had normalized.) The mass of these areas could be estimated, since we knew the volume of myocardium in between the epicardial and endocardial surfaces.

## Computing Anatomic Mass at Risk

The likely area at risk based on the anatomic data (coronary arteries) is that region of the myocardium supplied by arteries
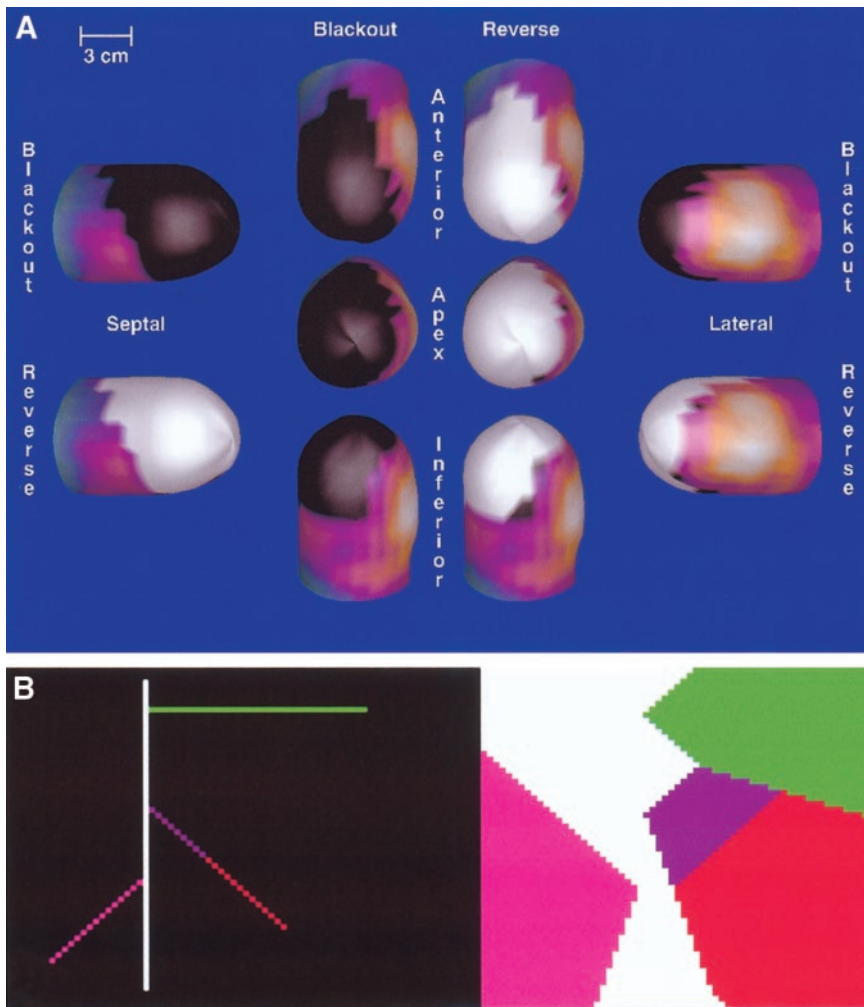
**FIGURE 3.** Physiologic and anatomic areas at risk. (A) Abnormal perfusion at stress (blacked-out regions) and areas that normalize at rest (whited-out regions). Whited-out regions are those that are at risk for myocardial infarction. In this patient population, blacked-out and whited-out areas are the same, since perfusion abnormality is in essence temporarily caused by the revascularization procedure, and revascularization then provides normal perfusion. This is same patient as shown in Figure 1. (B) Territories of left ventricle supplied by each coronary artery. Left and right pictures should be superimposed but are separated for sake of clarity. The left picture shows coronary artery as it would look if the left ventricle were flattened into 2D plane. Regions shown on the right picture are those areas that are closer to the artery of the same color than to any other artery. Thus, the green area in the right picture is supplied by the green artery in the left picture. The red area in the right picture corresponds to the portion of the artery that has had an occlusion placed in it. Thus, this is the area at risk for myocardial infarction, as determined by this model of coronary arteries and their territories. Mass of this area is then computed to obtain anatomic mass at risk.

distal to the stenosis. This region depends on knowledge of the LV territories supplied by each artery. Based on work by Seiler et al. (5), we define the territory of any coronary artery as those points on the left ventricle that are closer to that coronary artery than to any other coronary artery. Thus, the anatomic area at risk is that area of the left ventricle that is closest to the occluded vessel than to any other artery. This is shown graphically in Figure 3B. Again, the mass of this area could be estimated, since we knew the volume of myocardium in between the epicardial and endocardial surfaces.

### Evaluation of Accuracy

For all patients, 3D models were created for the LV and coronary artery tree. The ICP procedure was applied to the 3D models, and the alignment results were quantitatively evaluated for accuracy by comparing the size and extent of the myocardial area at risk as measured by perfusion to the area at risk as measured by anatomy. As described, the area of the blacked-out region of the myocardium as evaluated by perfusion quantification was considered the physiologic area at risk. The area of the myocardial territory supplied by coronary arteries distal to the occlusion was considered the anatomic area at risk. Because, in these carefully controlled acquisitions, the anatomic area at risk is directly related to the alignment of the LV and coronary arteries, the overlap of physiologic with anatomic area at risk is a measure of unification accuracy (Fig. 4). In this work, area and mass are directly proportional, since we assume a

1-cm-thick myocardium; therefore, we actually report mass-at-risk overlap, since it is a more common measure.

Two additional assessments of unification accuracy were performed. A linear regression between anatomic and physiologic
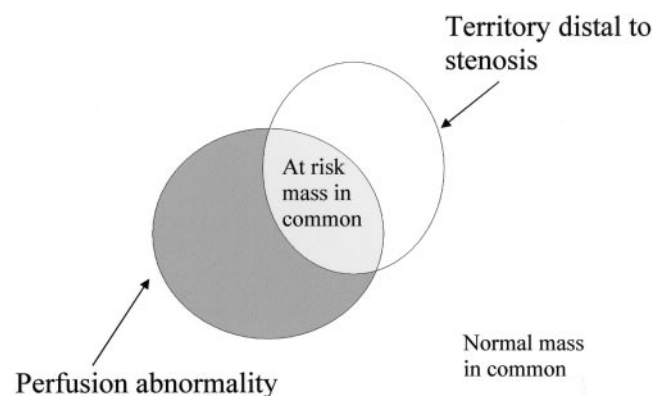


**FIGURE 4.** Mass at risk can be measured by perfusion abnormalities alone (physiologic mass at risk) and by coronary anatomy alone (anatomic mass at risk). Because in this study, we have induced the perfusion abnormality by creating anatomic occlusion in patients with single-vessel disease, these regions should overlap. Any error in overlap may be attributed to errors in unification.
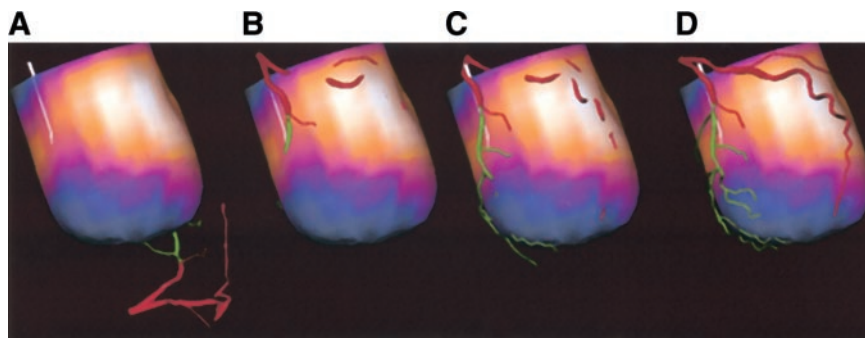
**FIGURE 5.** Successive steps of unification on patient study. Epicardial surface is color coded for perfusion. White line indicates anterior interventricular groove. (A) Original artery tree and epicardial surface positions. (B) Alignment after initial positioning. (C) Registration after ICP algorithm. (D) Final alignment after nonlinear warping.

mass at risk was computed, without regard to overlap. In addition, branch lengths of the coronary artery trees distal to the occlusion were correlated with physiologic mass at risk. This final relationship is similar to that suggested by Seiler et al. (*5*), who showed it to be linear in a canine model.

## RESULTS

An example of the results of unification at each step of the automatic process is shown in Figure 5. Note the successive improvement at each step.

In the 17 patients with LAD occlusions, the mean percentage of mass-at-risk overlap was 83% ± 17%. The mean percentage of normal mass overlap was 85% ± 8%. In the 6 patients with left circumflex artery (LCx) occlusions, the mean percentage of mass-at-risk overlap was 57% ± 25%. The mean percentage of normal mass overlap was 80% ± 10%. In the 7 patients with RCA occlusions, the mean

percentage of mass-at-risk overlap was 80% ± 8%. The mean percentage of normal mass overlap was 85% ± 4%. Overall, considering all 3 coronary distributions, mass-at-risk overlap was 80% ± 19%. The overall normal mass overlap was 84% ± 8%. Examples of patients for each type of occlusion (LAD, LCx, and RCA) are shown in Figure 6.

The anatomic mass at risk for these 30 patients was correlated with the physiologic mass at risk. The results are shown in Figure 7. The relationship between the 2 measurements was $y = 0.92x + 10.3$ g; $r = 0.76$; SEE = 10.4 g. The relationship between coronary artery branch length distal to the occlusion with physiologic mass at risk was $y = 0.1x + 17.6$ g; $r = 0.62$; SEE = 10.3 g.

The clinical utilization of a new software technique is always affected by its running time. All of the processing described in this work was on a Sun SPARC Ultra 1 computer with a 167-MHz processor and 128 Mb of mem-
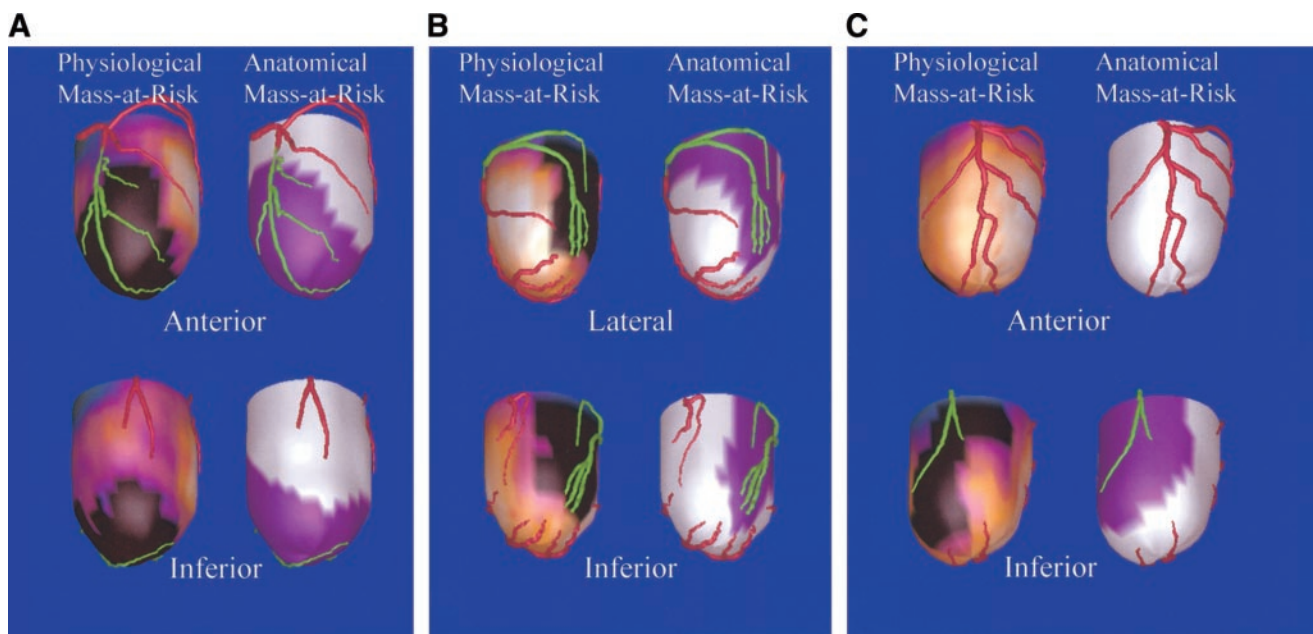


**FIGURE 6.** Unified models from patients with LAD stenosis (A), LCx stenosis (B), and RCA stenosis (C). For each example, 2 views are shown (top and bottom), and both 3D blackout maps and 3D anatomic mass-at-risk maps are shown for each view. Black regions on blacked-out model indicate those regions that are at risk based on perfusion information alone. Purple regions on at-risk models indicate those regions that are at risk based on coronary artery anatomy and its registration with epicardium. Overlap of black and purple regions indicates goodness of unification.
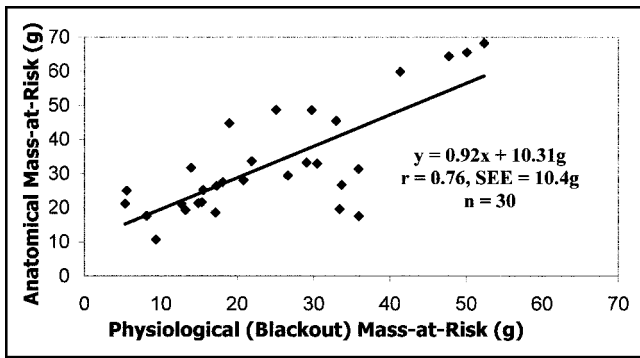
**FIGURE 7.** Anatomic mass at risk computed from coronary artery anatomy vs. physiologic mass at risk computed from perfusion quantification.

ory (Sun Microsystems), slow by today's speeds. The mean time required for alignment, including reading the coronary artery data files and displaying the 3D models, was $9 \pm 2$ s. This time was proportional to the size of the coronary artery model, which in turn was dependent on how many coronary artery branches were reconstructed.

## DISCUSSION

The primary goal of this study was to assess the performance of the fusion of the 3D coronary vascular tree onto the 3D myocardial perfusion distribution by comparing the location of single-vessel occlusion with the corresponding hypoperfused region. Evaluating the accuracy in patients is problematic because of the difficulty in determining the truth. An optimal validation requires visualization of both the vessels and the epicardial surface in a single study—for example, MRI for the left ventricle coupled with magnetic resonance angiography for coronary arteries. Unfortunately, such images are neither generally available nor clinically cost-effective. Previously, we have used visual analysis in animal models to compute goodness-of-fusion accuracy (13); however, visual techniques are neither reproducible nor objective. In this study, though, the patient data are extraordinarily well suited to evaluate the accuracy of the fusion objectively. In these subjects, there is a single and complete occlusion of a coronary artery with no collaterals and a single and well-defined perfusion abnormality in the SPECT study. Thus, the physiologic area at risk is by definition the result of the anatomic area at risk in this population, and the territories should overlap exactly if every portion of the algorithm performed correctly. We have previously validated both the perfusion quantification, 3D surface modeling of the left ventricle from SPECT (3,6,14), and the 3D reconstructions of the coronary arteries (9). Thus, the automatic alignment is the primary factor that affects the overlap of the anatomic and physiologic areas, or masses at risk.

Our results demonstrate that, in our selected population, the anatomic area at risk agrees well with the location and extent of the physiologic area at risk, as measured by

overlap. We have also demonstrated that the mass supplied by a coronary artery correlates well with the mass of the resulting perfusion abnormality in vivo, with $y = 0.92x + 10.3$ ($r = 0.76$). Our correlation of in vivo mass at risk with branch lengths distal to a stenosis is significantly lower ($y = 0.1x + 17.6$ g; $r = 0.62$). Note that the correlation of physiologic mass at risk with anatomic mass at risk may be high even if fusion is not particularly good; however, such a case is unlikely unless the error in fusion is a simple translation or a rotation about the long axis. A small error in alignment—for example, a simple translation or rotation about the long axis—may not affect the correlation. However, because of the warping process, a poorly aligned coronary artery tree would not provide a very accurate measurement of anatomic mass at risk, since the appearance of the tree on the left ventricle would be distorted. Also, because the left and right trees are aligned independently, alignment errors would need to be similar in both trees, or the relative size of the territories supplied by both would change. This is in fact the case with 2 subjects for whom the anatomic mass at risk was much less than the physiologic mass at risk. In contrast, the correlation of physiologic mass at risk with coronary artery lengths is primarily a measure of how well the coronary arteries themselves were detected and reconstructed. We included this measurement for comparison with the work of others.

Previously, Seiler et al. (5) demonstrated that the mass of muscle supplied by an arterial bed, defined as those myocardial points closer to the artery than to any other arterial branches, correlates well with microsphere data in ex vivo left ventricles, with $y = 0.93x + 5.53$ g. We have confirmed those findings in in vivo left ventricles. Seiler et al. demonstrated a much better correlation than we did when comparing ex vivo mass at risk with distal branch lengths ($y = 1.16x + 8.66$ g; $r = 0.98$). This is because we could not reconstruct greater than second-generation coronary artery branches. In contrast, Seiler et al. considered all visible branches, up to the third generation. However, the parameters of our regression relationships show the same trends as those published by Seiler et al.

Schindler et al. (4) also developed and implemented a methodology to fuse the 3D reconstructed coronary tree and 3D myocardial perfusion distribution. These investigators used the patient positioning information and detector placement exclusively to align the 2 structures; however, precise information about patient position is rarely available in the clinic. Their validation consisted of imaging a perfusion phantom with a tin-wire arterial structure, similar to our previous work (9). In applying this fusion technique, they subjectively assessed that 74% of 162 coronary lesions from 78 patients showed good coincidence with regional hypoperfusion.

In our results, the accuracy was best with LAD fusions and worst with LCx fusions. There are several reasons for this. First, the defects, as measured by physiologic mass at risk, were smaller in the LCx patients (8.3 g for LCx vs.

25.8 g for LAD and 13.2 g for RCA). Small defects may underestimate mass-at-risk overlap as described in the Limitations section. Also, proper alignment of the LCx with the myocardial surface is very dependent on accurate groove identification. Rotational errors in alignment may result in only minimal overlap, especially as the defects in these patients were small.

The special characteristics of the datasets in this particular problem make registration quite difficult. Because the dimensionalities of the images are different, and because they do not even display the same structures, image-based alignment techniques cannot be used. The low resolution of the SPECT data makes identification of landmarks quite difficult as well. Thus, our technique focused on using the objects themselves, and a surface-based approach appeared to be the most fitting for this application. The ICP algorithm was chosen because it requires no extracted features, no curve or surface derivatives, and no preprocessing of 3D data. Thus, it is expected to be fast. We have further streamlined the algorithm to make use of the fact that the epicardium is a (nearly) convex surface—that is, a line drawn from the center of mass of the surface will intersect the surface in only one place. The resulting unification times demonstrate the efficiency of this algorithm. In addition, Besl and Mckay (11) proved that the ICP registration converges to a local minimum of the cost function (which minimizes the mean square distance between the arteries and the left ventricle); thus, problems with divergence of the iterative algorithm can in practice be avoided.

### Clinical Applications

There are several major expected clinical applications of the automatic fusion procedure validated by this work. One is to fuse the perfusion and angiographic information during coronary arteriography as an image-guided gantry positioning system. This approach could identify optimal gantry positioning for stenotic lesions that are difficult to see from the arteriogram alone but that result in hypoperfused regions. In the setting of a patient with multiple-vessel disease, the fused model could also assist in locating and assessing the physiologic significance and severity of stenotic lesions to undergo reperfusion first. Another clinical application is to use this fusion in either the catheterization laboratory or the nuclear cardiology laboratory in patients for whom the anatomic and physiologic area at risk do not agree as a sign of collaterals or microcirculatory disease. Clearly, not all patients receive both SPECT and angiography; however, both tests are more likely to be performed in particularly difficult clinical cases. In those patients, fusion of the information of the 2 studies may be even more important. Also, as new technologies are developed that are capable of performing both studies in a single examination—for example, PET/CT machines—it is likely that more patients will receive both perfusion and angiography studies. In fact, our work is applicable to images acquired by PET/CT machines, since much of the data processing is essentially the same, but the fusion operation will be less complicated, due to the near-alignment of PET and CT images acquired on a PET/CT scanner.

### Limitations

One limitation of this study is that the search for collateral vessels was performed on the basis of detecting spontaneously visible coronary collaterals during coronary angiography. This approach does not totally exclude the presence of coronary collateral circulation. This limitation accounts for some of the error in correlating the anatomic and physiologic mass at risk independent of the error of the fusion algorithm. More accurate techniques for detecting collateral flow could have been used, such as using sensor-tipped angioplasty guide wires to measure pressure or flow velocity distal to the site of the balloon occlusion. These techniques were not considered because of the complexity (and thus time and risk) that they would have added to the angioplasty procedure in this population of patients with a single coronary lesion.

Because the ICP algorithm finds a local minimum dependent on the starting position of the models, the initial positioning of the 2 objects is important. More work needs to be done to determine the sensitivity of the registration to small changes in the starting point.

The use of mass at risk to validate alignment does have some drawbacks. In general, the more distal a defect is the more informative it is regarding unification accuracy (e.g., note the converse case for the RCA examples). However, the smaller the mass at risk is, the less likely there is to be a large amount of overlap. Also, in the case of a small mass at risk, a "near miss" may be quite useful clinically but will be judged as a 0% mass-at-risk overlap by this assessment. Conversely, the larger the mass at risk is, the more likely there is to be a high percentage of overlap. Thus, small defects tend to skew results toward a lower mass-at-risk overlap and higher normal mass overlap; larger defects skew results toward a higher mass-at-risk overlap and reduced normal mass overlap. This may be one reason we see a relatively low normal mass overlap in this study, since most occlusions were placed rather proximally in the coronary artery tree.

### Improvements

All steps in the unification process were performed automatically. The interventricular groove detection and initial alignments were not adjusted by the user. In a truly clinical setting, these variables should be modified by a user whenever the automatic algorithms do not provide the best answer. The use of operator assistance may have improved our results, particularly in the case of large defects that obliterate the insertion of the right ventricle into the left ventricle. This can cause errors in the automatic groove-finding algorithm and affect the angular position of the artery tree. Although overlap of physiologic with anatomic mass at risk seems to be a valid approach for assessing the accuracy of unification, it may not provide a good measure

of the clinical utility of the technique. A large prospective trial is required to document the clinical value of the automatic fusion approach for correlating physiologic and anatomic information over the subjective approaches used today.

## CONCLUSION

A unification algorithm for automatically registering 3D models of the epicardial surface from perfusion SPECT and 3D coronary artery trees from coronary angiography has been presented. Its performance has been evaluated by using a unique patient study in which anatomic and physiologic areas at risk should overlap. In this population, we were able to obtain a high degree of overlap and thus validate the accuracy of the unification process.

## ACKNOWLEDGMENTS

## REFERENCES

1. Klein JL, Hoff JG, Peifer JW, et al. A quantitative evaluation of the three dimensional reconstruction of patients coronary arteries. *Intl J Cardiovasc Imaging.* 1998;14:75–87.

2. Messenger JC, Chen SY, Carroll JD, et al. 3D coronary reconstruction from routine single-plane coronary angiograms: clinical validation and quantitative analysis of the right coronary artery in 100 patients. *Int J Cardiovasc Imaging.* 2000;6:413–427.

3. Faber TL, Cooke CD, Peifer JW, et al. Three-dimensional displays of the left ventricular epicardial surface from standard cardiac SPECT perfusion quantification techniques. *J Nucl Med.* 1995;36:697–702.

4. Schindler TH, Magosaki N, Jeserich M, et al. Fusion imaging: combined visualization of 3D reconstructed coronary artery tree and 3D myocardial scintigraphic image in coronary artery disease. *Int J Cardiovasc Imaging.* 1999;15: 357–368.

5. Seiler C, Kirkeeide RL, Gould KL. Measurement from arteriograms of regional myocardial bed size distal to any point in the coronary vascular tree for assessing anatomic area at risk. *J Am Coll Cardiol.* 1993;21:784–797.

6. Garcia EV, Cooke CD, Van Train KF, et al. Technical aspects of myocardial SPECT imaging with technetium-99m sestamibi. *Am J Cardiol.* 1990;66:23E–31E.

7. Duijves P. *Floating Volume: A New Approach for Segmentation of Cardiovascular Trees* [master's thesis]. Delft, The Netherlands: Delft Technical University; 1997.

8. Reiber JHC, Surruys PW. Quantitative coronary angiography. In: Marcus M, ed. *Cardiac Imaging: A Companion to Braunwalds Heart Disease.* Philadelphia, PA: Elsevier Science; 1990:211–280.

9. Peifer JW, Ezquerra NF, Cooke CD, et al. Visualization of multimodality cardiac imagery. *IEEE Trans Biomed Eng.* 1990;37:744–756.

10. Faber TL, Chiron F, Ezquerra NF, et al. Registration of multimodal 3D cardiac information using the iterative closest point approach. In: Wilson DC, Tagare HD, Bookstein FL, et al., eds. *Mathematical Modeling, Estimation, and Imaging.* Proceedings SPIE 4121. Bellingham, WA: SPIE; 2000:233–241.

11. Besl PJ, Mckay ND. A method for registration of 3-d shapes. *IEEE Trans Pattern Anal Mach Intell.* 1992;14:239–256.

12. Kim Y, Aggarwal JK. Determining object motion in a sequence of stereo images. *IEEE Trans Rob Autom.* 1987;3:599–614.

13. Faber TL, Peifer JW, Klein JL, et al. Automated unification of three-dimensional models of the left ventricular epicardium and coronary artery tree. *IEEE Comput Cardiol.* 1996;333–336.

14. Faber TL, Cooke CD, Folks RD, et al. Left ventricular function and perfusion from gated SPECT perfusion images: an integrated method. *J Nucl Med.* 1999; 40:650–659.